Journal of Marine Science and Application (2025) 24: 1019-1026
https://doi.org/10.1007/s11804-024-00501-7

RESEARCH ARTICLE

Computing the Far-Field Scattered by a Spherical Target Near the Seabed

Natalie S. Grigorieva[1], Fiodor F. Legusha[1] and Kirill S. Safronov[1]

Received: 27 March 2024 / Accepted: 30 July 2024

Abstract

This study proposes a numerically efficient technique for computing the far-field scattered by a spherical target placed near the seabed. The bottom is supposed to be a homogeneous liquid attenuating half-space. The transmitter and receiver are situated at different points of a homogeneous water half-space. The distances between the transmitter, receiver, and object of interest are assumed to be much larger than the acoustic wavelength in water. The scattered far-field is ascertained using Hackman and Sammelmann's general approach. The arising scattering coefficients of a sphere are assessed using the steepest descent approach. The branch cut contribution is also considered. The obtained formulas for the form-function can be used for acoustically rigid or soft scatterers, as well as elastic targets or spherical elastic shells. Numerical simulations are conducted for an acoustically rigid sphere. Asymptotic expressions for the scattering coefficients allow a decrease in the number of summands in the formula for the target strength and a significant reduction in computational time.

Keywords Scattering of acoustic waves; Spherical scatterer; Attenuating liquid bottom; Later wave; Target strength

1 Introduction

Acoustic scattering by a spherical target located near a plane boundary is an important concern in various practical applications. Many publications on this subject can be found in (Gaunaurd and Huang, 1994; Gaunaurd and Huang, 1995; Huang and Gaunaurd, 1996; Hickling, 1964; Fawcett et al., 1998; Zampolli et al., 2008; 2009).

This study is devoted to computing the far-field scattered by a spherical target near the attenuating liquid bottom. This medium model regards such real phenomena as bottom penetration by the acoustic waves. The scattered field is ascertained using Hackman and Sammelmann's general approach (Hackman and Sammelmann, 1986; Hackman and Sammelmann, 1988). This approach is based on the *T*-matrix formalism and is applicable for acoustically rigid or soft scatterers, as well as elastic targets or spherical elastic shells. In this study, numerical simulations are conducted for an acoustically rigid target.

The total field scattered by a spherical target is represented as the sum of the solution in a medium without a target and the summand describing the scatterer contribution. In turn, the scatterer contribution is the sum of summands−scattering coefficients. Each of these summands is an integral with an integrand including special functions: the Hankel spherical functions and the associated Legendre functions. Along the infinite interval of integration, the integrand of scattering coefficients is a slowly decreasing and fast oscillating function. At the frequencies considered in the numerical example in this study, the scatterer contribution includes $O(10^3)$ scattering coefficients. As a result, the computing of the far-field scattered by a spherical target near the attenuating seabed becomes rather time consuming.

In this study, the scattering coefficients are assessed using the steepest descent method (Brekhovskikh, 1980; Brekhovskikh and Godin, 1990). The branch cut contribution is considered as well. The use of these asymptotic expansions for the scattering coefficients and the addition theorem for the associated Legendre functions enables a decrease in the number of summands in the formula for the scatterer contribution by approximately 10 times at the frequencies considered in the numerical example. After these transformations, the summands in the formula for the scatterer contribution only include elementary functions without their integration.

This numerically efficient technique for computing the field scattered by a spherical target near the attenuating

Article Highlights

- A numerically efficient technique is introduced for calculating far-filed scattering by a spherical target near the seabed.
- The method efficiently handles acoustically rigid, soft scatterers, elastic targets, and spherical elastic shells.
- Asymptotic expressions for scattering coefficients enable a reduction in computational complexity and time.

✉ Kirill S. Safronov
safronov.kirill.pm@gmail.com

[1] Saint Petersburg State Marine Technical Department, University of Physics, Saint Petersburg, 190121, Russia

bottom and for the buried scatterer was proposed in (Grigorieva et al., 2016; Grigorieva et al., 2023) for the case of echo-signal. In the present study, this technique is generalized to the case when the transmitter and receiver are located at two different points of a homogeneous water half-space.

An alternative and potentially attractive approach for computing the scattering coefficients of a sphere is the method of complex images (Nobile and Hayek, 1985; Fawcett, 2000; Fawcett, 2003; Fawcett and Lim, 2003; Ochmann, 2004; Taraldsen, 2005). The complex image solution is based on the approximation of the reflection coefficients via a discrete sum of image point sources with complex source point coordinates. This method offers validity in the near field and the existance of a simple recursion relation in frequency (Fawcett, 2003) for computing source parameters.

This study aims to comprehensively investigate the far-field scattered by a spherical target close to the attenuating seabed. Thus, the present study is focused on the steepest descent approximation of the scattering coefficients of a sphere.

All computations and plots in this study are performed using the computer algebra system Wolfram Mathematica. For special functions, such as the spherical Hankel functions or Legendre polynomials, the built-in functionality is adopted.

The rest of the paper is organized as follows. In Section 2, we propose a numerically efficient technique for computing the far-field scattered by a spherical target located close to the seabed. In Section 3, the modeling of the target strength is conducted and discussed. Section 4 summarizes the relevant points. Section 5 elaborates on the conclusions.

2 Simulation of the total far-field scattered by a spherical target located near the seabed

Throughout the entire study, the attention is restricted to harmonic oscillations of constant frequency f. The complex time dependence $\exp(\mathrm{i}\omega t)$, with t representing time, $\mathrm{i} = \sqrt{-1}$, and $\omega = 2\pi f$, is factored out of the equations.

The origin of coordinates is placed at the center of a spherical scatterer of a radius a. The Oz axis is directed vertically upwards as shown in Figure 1. The scatterer is immersed in a water half-space, which has a density ρ and sound speed c and occupies the half-space $z > -b$. The bottom has a density ρ_b and sound speed c_b and occupies the half-space $z < -b$. The weak attenuation in the bottom is accounted for by introducing the complex sound index of refraction

$$n = \frac{c}{c_b}(1 + \mathrm{i}\delta), \delta > 0 \tag{1}$$

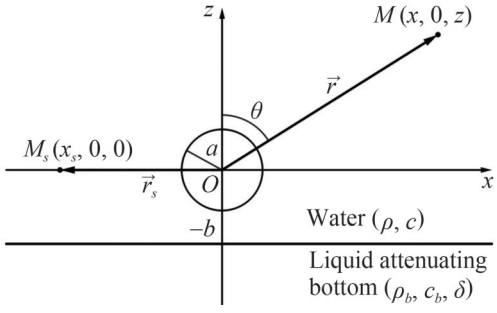

Figure 1 Scattering geometry (not to scale)

A point source emitting the spherical wave with a cyclical frequency ω is located at the point M_s of the water half-space. The Cartesian and spherical coordinates of the point M_s are $(x_s, 0, 0)$, $x_s < 0$, and $(r_s, \theta_s, \varphi_s)$, where $\theta_s = \pi/2$ and $\varphi_s = \pi$. A receiver is located at the point M of the water half-space. The Cartesian and spherical coordinates of the point M are $(x, 0, z)$ and (r, θ, φ), respectively, where $x > 0$ and $\varphi = 0$.

Using the method proposed by Hackman and Sammelmann (1986, 1988), the total scattered field Φ_{total} can be found as the sum of the source Φ_{src} and scatterer Φ_{scat} contributions:

$$\Phi_{\text{total}} = \Phi_{\text{src}} + \Phi_{\text{scat}} \tag{2}$$

If $z > z_s$, then the source contribution is defined as

$$\Phi_{\text{src}} = \frac{\mathrm{i}}{4\pi}\int_0^\infty \frac{qdq}{h} J_0\left(q\left|x - x_s\right|\right) \times\left(\mathrm{e}^{\mathrm{i}h(z - z_s)} + V(q)\mathrm{e}^{\mathrm{i}h(z + 2b + z_s)}\right) \tag{3}$$

Here, J_0 is the zero-order Bessel cylindrical function, q and $h = h(q) = \sqrt{k^2 - q^2}$ are the horizontal and vertical components of the incident wave vector in water, and $k = \omega/c$ is the wave number. The coefficient of reflection from the bottom $V(q)$ (Brekhovskikh and Godin, 1990) is

$$V(q) = \frac{\eta h - h_b}{\eta h + h_b} \tag{4}$$

where $\eta = \rho_b/\rho$, $h_b = h_b(q) = \sqrt{k_b^2 - q^2}$, $k_b = \omega/c_b$ is the wave number in the liquid bottom. The inequalities $\mathrm{Im}\, h(q) \geqslant 0$ and $\mathrm{Im}\, h_b(q) \geqslant 0$ are assumed to be satisfied on the complex q plane.

If $z_s > z$, then Φ_{src} is defined by the equation derived from Eq. (3) by swapping z and z_s.

The scatterer contribution is defined as

$$\Phi_{\text{scat}} = -\frac{\mathrm{i}}{k}\sum_{l=0}^{\infty} T_l \sum_{m=0}^{l} A_{ml}(\boldsymbol{r}) C_{ml}(\boldsymbol{r}_s) \tag{5}$$

In Eq. (5), T_l represents the elements of the free-field

T-matrix for acoustical scattering by the considered target. These elements are found using the separation of variables and applying the appropriate boundary conditions to the spherical harmonics. For the acoustically rigid sphere of a radius a, we have

$$T_l = -\frac{j_l'(ka)}{h_l^{(1)\prime}(ka)} \tag{6}$$

where $j_l(x)$ is the spherical Bessel function, $h_l^{(1)}$ is the spherical Hankel function of the first kind, and the prime marking the spherical functions indicates a derivative with respect to the entire argument. The T-matrix for a spherical elastic shell filled with air can be found in Appendix A of (Grigorieva and Fridman, 2013).

The scattering coefficients of a sphere $A_{ml}(\boldsymbol{r})$ are as follows:

$$A_{ml}(\boldsymbol{r}) = \mathrm{i}^{l-m+1}\sqrt{\frac{\varepsilon_m}{2\pi}}\cos m\varphi\left\{(-1)^{m+l}\int_0^\infty \frac{qdq}{h}J_m(q|x|)\times\Pi_l^m\left(\frac{h}{k}\right)\mathrm{e}^{\mathrm{i}hz} + \int_0^\infty \frac{qdq}{h}J_m(q|x|)V(q)\Pi_l^m\left(\frac{h}{k}\right)\mathrm{e}^{\mathrm{i}h(2b+z)}\right\}$$
$$= \cos m\varphi\left\{A_{ml}^{(f)}(\boldsymbol{r}) + A_{ml}^{(d)}(\boldsymbol{r})\right\} \tag{7}$$

Here, $\varepsilon_0 = 1$ and $\varepsilon_m = 2$ for $m \geqslant 1$, J_m is the cylindrical Bessel function of the mth order, and $\Pi_l^m(x)$ represents the normalized Legendre functions of the order l and rank m (Bateman and Erdélyi, 1953):

$$\Pi_l^m(x) = \sqrt{\frac{2l+1}{2}\frac{(l-m)!}{(l+m)!}}P_l^m(x)$$

In this study, we use the single-scatter approximation when $C_{ml}(\boldsymbol{r}_s) = A_{ml}(\boldsymbol{r}_s)$. The full multiple scattering solution modeling the backscattered field from a thin air-filled spherical elastic shell in a water half-space close to the seabed was studied in (Sessarego et al., 2012).

If the scattered field is evaluated with the full multiple scattering, then the coefficients $C_{ml}(\boldsymbol{r}_s)$ in Eq. (5) are found using a linear system of algebraic equations (Hackman and Sammelmann, 1986; Hackman and Sammelmann, 1988). In this system, the coefficients are integrals with slowly decreasing and rapidly oscillating integrands. As a result, the computing of the coefficients $C_{ml}(\boldsymbol{r}_s)$ becomes rather time consuming. Therefore, in this study, we consider the single-scatter approximation.

The trancation level $l_{\max}$ in Eq. (5) is set by a rule suggested in (Kargl and Marston, 1990)

$$l_{\max} = \left[ka + 4.05(ka)^{\frac{1}{3}}\right] + 3 \tag{8}$$

where $[x]$ is the integer part of x. For $a = 0.3$ m, $c = 1\,500$ m/s, and $f = 60$ kHz, Eq. (8) yields $l_{\max} = 95$. Thus, for computing the scattered field (5), summing up more than 4 500 summands is necessary.

The integral $A_{ml}^{(f)}(\boldsymbol{r})$ (Eq. (7)) can be calculated in explicit form (Hackman and Sammelmann, 1988):

$$A_{ml}^{(f)}(\boldsymbol{r}) = \mathrm{i}k\sqrt{\frac{\varepsilon_m}{2\pi}}h_l^{(1)}(kr)\Pi_l^m(\cos\theta) \tag{9}$$

Using the main term of the asymptotic expansion for $h_l^{(1)}(kr)$ as $kr \gg 1$, we obtain

$$A_{ml}^{(f)}(\boldsymbol{r}) \sim \frac{1}{r}\sqrt{\frac{\varepsilon_m}{2\pi}}\Pi_l^m(\cos\theta)\mathrm{e}^{\mathrm{i}\left(kr-\frac{\pi l}{2}\right)} \tag{10}$$

The integral $A_{ml}^{(d)}(\boldsymbol{r})$ is calculated in explicit form only if the reflection coefficient $V(q)$ does not depend on q.

The integral representation of the scattering coefficients (7) is valid for arbitrary frequencies and distances between the observation point and the target. At frequencies of interest of 40–60 kHz and distances of 50–100 m considered in this study, the integrand in (7) is rapidly oscillating and slowly decreasing. This condition makes the straightforward calculation of the scattering coefficients rather time consuming. To speed up the computation of the integrals (5), we evaluate them using the steepest descent method (Brekhovskikh, 1980; Brekhovskikh and Godin, 1999).

Following (Grigorieva et al., 2016), in the main approximation with respect to kr_d:

$$A_{ml}^{(d)}(\boldsymbol{r}) \sim (-1)^m\sqrt{\frac{\varepsilon_m}{2\pi}}\frac{1}{r_d}\Pi_l^m(\cos\theta_d)U(\theta_d)\mathrm{e}^{\mathrm{i}\left(kr_d-\frac{\pi l}{2}\right)} \tag{11}$$

Here,

$$r_d = \sqrt{x^2 + (2b+z)^2},\ \theta_d = \arctan\frac{x}{2b+z},$$
$$\cos\theta_d = \frac{2b+z}{r_d} \tag{12}$$

$$U(\alpha) = \frac{\eta\cos\alpha - \sqrt{n^2 - 1 + \cos^2\alpha}}{\eta\cos\alpha + \sqrt{n^2 - 1 + \cos^2\alpha}} = V(k\sin\alpha) \tag{13}$$

Asymptotic formula (11) loses its meaning if $n^2 - \sin^2\theta_d \to 0$. The reason is that the steepest descent method assumes that the reflection coefficient $U(\alpha)$ is a slowly changing function. Meanwhile, if the angle θ_d is close to the angle of the total internal reflection $\alpha_* = \arcsin c/c_b$,

then the first and the second derivatives of $U(\alpha)$ tend to infinity.

In the region $\theta_d > \alpha_*$, if $c/c_b < 1$, then the two-valuedness of function $U(\alpha)$ needs to be considered. Owing to this two-valuedness in the expression for $A_{ml}^{(d)}(\boldsymbol{r})$, an additional term $\hat{A}_{ml}^{(d)}(\boldsymbol{r})$ appears in the right-hand side of Eq. (11). It corresponds to the branch cut contribution. The formula for this term was obtained in (Grigorieva et al., 2016):

$$\hat{A}_{ml}^{(d)}(\boldsymbol{r}) \sim (-1)^{m+1} \sqrt{\frac{\varepsilon_m}{2\pi}} \frac{\Pi_l^m(\cos\theta_d)}{kr_d^2} \chi(\alpha_*, \theta_d) \times \exp\left[\mathrm{i}kr_d \cos(\alpha_* - \theta_d) - \frac{\mathrm{i}\pi l}{2} \right] \tag{14}$$

where

$$\chi(\alpha_*, \theta_d) = \frac{2n}{\eta \sqrt{\cos\alpha_* \sin\theta_d} \left[\sin(\alpha_* - \theta_d) \right]^{\frac{3}{2}}} \tag{15}$$

Formula (14) loses its meaning if $\theta_d \to \alpha_*$ and for $\mathrm{Re}\, n \to 1$ because $\cos\alpha_* = \sqrt{1 - \sin^2\alpha_*} = \sqrt{1 - (\mathrm{Re}\, n)^2}$. As discussed in Brekhovskikh (1980), Brekhovskikh and Godin (1999) for a classical lateral wave, it is possible to prove that Eq. (14) is valid if $kr_d(\theta_d - \alpha_*)^2 \gg 1$.

For $A_{ml}(\boldsymbol{r}_s)$, formulas similar to (9)–(15) can be obtained. In this case, the following distances and angles appear:

$$r_s = |x_s|,\ \theta_s = \frac{\pi}{2},\ r_{s,d} = \sqrt{x_s^2 + (2b)^2},$$
$$\theta_{s,d} = \arctan\frac{|x_s|}{2b},\ \cos\theta_{s,d} = \frac{2b}{r_{s,d}} \tag{16}$$

With the obtained asymptotic expressions for $A_{ml}(\boldsymbol{r})$ and $A_{ml}(\boldsymbol{r}_s)$, the number of summands in Eq. (5) can be essentially reduced with the use of the addition theorem for the associated Legendre functions (Bateman and Erdélyi, 1953):

$$P_l(\cos\varphi_1) P_l(\cos\varphi_2) + 2 \sum_{m=1}^{l} \frac{\Gamma(l-m+1)}{\Gamma(l+m+1)} P_l^m(\cos\varphi_1) \times P_l^m(\cos\varphi_2) \cos m\beta = P_l(\cos\varphi_1 \cos\varphi_2 + \sin\varphi_1 \sin\varphi_2 \cos\beta) \tag{17}$$

where $0 \leqslant \varphi_1 < \pi$, $0 \leqslant \varphi_2 < \pi$, $\varphi_1 + \varphi_2 < \pi$, β is a real number, P_l is the Legendre polynomial of degree l, and Γ is the gamma-function.

For example, if $\theta_d < \alpha_*$ and $\theta_{s,d} > \alpha_*$, then we obtain

$$\sum_{m=0}^{l} (-1)^m \left[A_{ml}^{(f)}(\boldsymbol{r}) + A_{ml}^{(d)}(\boldsymbol{r}) \right] \times A_{ml}^{(f)}(\boldsymbol{r}_s) + A_{ml}^{(d)}(\boldsymbol{r}_s) + \hat{A}_{ml}^{(d)}(\boldsymbol{r}_s) \Big] = A^{(f,f)} + A^{(f,d)} + \hat{A}^{(f,d)} + A^{(d,f)} + A^{(d,d)} + \hat{A}^{(d,d)} \tag{18}$$

Here,

$$A^{(f,f)} \sim \frac{2l+1}{4\pi r r_s} P_l\left(\cos(\theta + \theta_s)\right) \mathrm{e}^{\mathrm{i}\left[k(r + r_s) - \pi l\right]} \tag{19}$$

$$A^{(f,d)} \sim \frac{2l+1}{4\pi r r_{s,d}} P_l\left(\cos(\theta - \theta_{s,d})\right) U(\theta_{s,d}) \mathrm{e}^{\mathrm{i}k(r + r_{s,d})} \tag{20}$$

$$\hat{A}^{(f,d)} \sim -\frac{2l+1}{4\pi k r r_{s,d}^2} P_l\left(\cos(\theta - \alpha_*)\right) \chi(\alpha_*, \theta_{s,d}) \times \mathrm{e}^{\mathrm{i}\left[kr + kr_{s,d}\cos(\alpha_* - \theta_{s,d}) - \pi l\right]} \tag{21}$$

$$A^{(d,f)} \sim \frac{2l+1}{4\pi r_d r_s} P_l\left(\cos(\theta_d - \theta_s)\right) U(\theta_d) \mathrm{e}^{\mathrm{i}k(r_d + r_s)} \tag{22}$$

$$A^{(d,d)} \sim \frac{2l+1}{4\pi r_d r_{s,d}} P_l\left(\cos(\theta_d + \theta_{s,d})\right) U(\theta_d) U(\theta_{s,d}) \times \mathrm{e}^{\mathrm{i}\left[k(r_d + r_{s,d}) - \pi l\right]} \tag{23}$$

$$\hat{A}^{(d,d)} \sim -\frac{2l+1}{4\pi k r_d r_{s,d}^2} P_l\left(\cos(\theta_d + \alpha_*)\right) \chi(\alpha_*, \theta_{s,d}) U(\theta_d) \times \mathrm{e}^{\mathrm{i}\left[kr_d + kr_{s,d}\cos(\alpha_* - \theta_{s,d})\right]} \tag{24}$$

The source contribution (3) is evaluated as

$$\Phi_{\mathrm{src}} \sim \frac{1}{4\pi R} \mathrm{e}^{\mathrm{i}kR} + \frac{1}{4\pi R_d} U(\Psi_d) \mathrm{e}^{\mathrm{i}kR_d} \tag{25}$$

where

$$R = |MM_s| = \sqrt{(x - x_s)^2 + z^2},$$
$$R_d = \sqrt{(x - x_s)^2 + (z + 2b)^2},$$
$$\Psi_d = \arctan\frac{x - x_s}{z + 2b},\ \cos\Psi_d = \frac{z + 2b}{R_d} \tag{26}$$

If $\Psi_d > \alpha_*$, then the right-hand side of Eq. (25) needs to be added a summand corresponding to the lateral wave contribution ((15)):

$$-\frac{\mathrm{i}}{2\pi k R_d^2} \chi(\alpha_*, \Psi_d) \exp\left[\mathrm{i}kR_d \cos(\alpha_* - \Psi_d)\right] \tag{27}$$

In the next section, the technique proposed above is used for the modeling of the target strength.

3 Numerical results for the acoustically rigid sphere

The technique proposed in Section 2 is illustrated here by considering an acoustically rigid scatterer of a radius $a = 0.3$ m. It is located in the water half-space $z > -b$ close to the attenuating liquid seabed $z < -b$, where $b = 5$ m. The origin of coordinates O coincides with the sphere center (Figure 1).

The water has the following properties: $\rho = 1\,000$ kg/m^3 $c = 1\,500$ m/s. The bottom has the following properties: $\rho_b = 1\,800$ kg/m^3 and $c_b = 1\,600$ m/s. In this case, the critical angle of reflection $\alpha_* = \arcsin c/c_b = 1.215\,4$ rad. The receiver is located at the point M. The Cartesian and spherical coordinates of this point are $(x, 0, z)$ and (r, θ, φ), respectively, where $\varphi = 0$, $\theta = 65° = 1.134\,5$ rad, and $y = 50$ m yield $z = 23.32$ m and $r = |OM| = 55.17$ m.

The attenuation in the bottom is considered by introducing the complex sound index of refraction (1) with $\delta = 0.01$.

A point source emitting a spherical wave with the cyclical frequency ω is located at the point M_s of the water half-space. The Cartesian and spherical coordinates of the point M_s are $(x_s, 0, 0)$ and $(r_s, \theta_s, \varphi_s)$, respectively, where $x_s = -100$ m, $\theta_s = \pi/2$, and $\varphi_s = \pi$.

The total scatterer field Φ_{total} is compared with the source contribution Φ_{src} (Eq. (2)) over the frequency band $40 \leqslant f \leqslant 60$ kHz using the technique proposed in Section 2. In this case, the lateral wave component should be considered in computing Φ_{src} because $\Psi_d = \arctan\dfrac{z+2b}{R_d} = 1.352\,2$ rad $> \alpha_*$, and $A_{ml}(\boldsymbol{r}_s)$, where $\theta_{s,d} = \arctan\dfrac{|x_s|}{2b} = 1.471\,1$ rad $> \alpha_*$.

The quantities of interest are the source strength

$$\text{TS}_{\text{src}} = 20\log_{10}\frac{|\Phi_{\text{src}}|}{|\Phi_{\text{ref}}|} \tag{28}$$

and the total strength

$$\text{TS}_{\text{total}} = 20\log_{10}\frac{|\Phi_{\text{total}}|}{|\Phi_{\text{ref}}|} \tag{29}$$

with the effect of the spherical target scattering;

$$\Phi_{\text{ref}} = \frac{e^{ikR_{\text{ref}}}}{4\pi R_{\text{ref}}} \tag{30}$$

where $R_{\text{ref}} = |x_0| = 100$ m.

Figure 2 illustrates the scattering from the acoustically rigid spherical target at $x = 50$ m. The dashed line corresponds to TS_{src} and the solid line to TS_{total}.

Approximate values of the source strength and the total strength obtained using (11)–(13) and (18)–(24) and the exact values calculated using (3)–(7) for attenuating sandy sediment are compared at several frequencies from the inverval $55 \leqslant ka \leqslant 60$. At all these points, the difference between them is of the order of 10^{-3}. Thus, the agreement between the exact and asymptotic formulas is excellent.

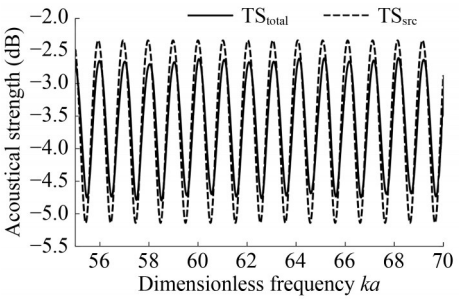

Figure 2 Dependence of the source strength TS_{src} (dashed line) and the total strength TS_{total} (solid line) on ka at $x = 50$ m

To compute integrals $A_{ml}^{(d)}(\boldsymbol{r})$ ((7)) at a fixed point from the interval $40 \leqslant f \leqslant 60$ kHz, we start with the equality obtained for the case $V = \text{const}$ in Hackman and Sammelman (1988):

$$A_{ml}^{(d)}(\boldsymbol{r}) = ik(-1)^{l+m}\sqrt{\frac{\varepsilon_m}{2\pi}}\,V\,h_l^{(1)}(kr_d)\Pi_l^m(\cos\theta_d)$$

where r_d and θ_d are given by (12). This equality allows finding the step of integration and the length of the integration interval to provide the required accuracy. Then, using these parameters, the integral $A_{ml}^{(d)}(\boldsymbol{r})$ itself (see (7)) is evaluated.

In Figures 3–5, the coordinates x equal 30, 20, and 10 m, respectively. Other parameters of the problem including the angle θ and $R_{\text{ref}} = |x_0|$ are the same as before. In all these cases, the angle Ψ_d is greater than α_*. Thus, in all these cases, the lateral wave should be considered while calculating Φ_{src}.

In all the cases, $x = 10$, 20, 30, 50 m, the receiver is located in the illuminated zone. Since the sphere is considered a rigid body, there is no wave propagating inside the

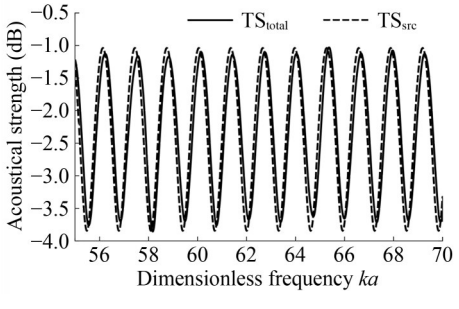

Figure 3 Dependence of the source strength TS_{src} (dashed line) and the total strength TS_{total} (solid line) on ka at $x = 30$ m

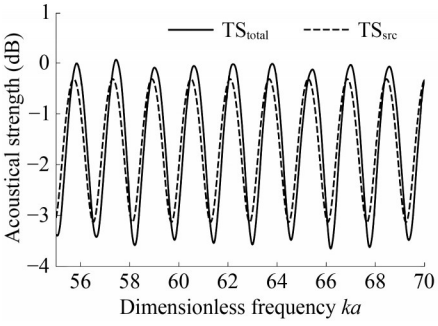

Figure 4 Dependence of the source strength TS_{src} (dashed line) and the total strength TS_{total} (solid line) on ka at x = 20 m

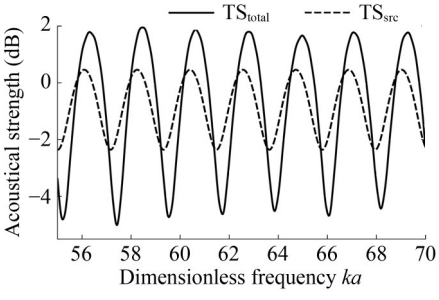

Figure 5 Dependence of the source strength TS_{src} (dashed line) and the total strength TS_{total} (solid line) on ka at x = 10 m

sphere (no elastic effects) and scattering problem reduces to a simple reflection problem in the exterior domain for the sphere. In this case, the received signal consists of three components: the direct wave, the wave reflected from the bottom, and the Franz creeping wave exited at the sphere boundary between the illuminated and shadowed parts of the sphere.

The case of acoustic scattering by an elastic spherical shell near the seabed was analyzed in detail in (Sessarego et al., 2012). Herein, computational results are obtained for a thin air-filled spherical elastic shell immersed in water close to the seabed or to air/water interface. Computational results obtained for the full multiple scattering solution are compared with the model utilizing the single-scatter approximation in a wide frequency range of $0 < ka < 55$. In this frequency range, for a thin air-filled spherical shell the main elastic contribution to scattering is due to the lowest-order compressional wave which is the generalization of the Lamb symmetric wave of a flat plate and due to the subsonic mode of the first antisymmetric Lamb wave. Strong resonance peaks produced by these waves in the backscattered form-function are identified in numerical modeling. As observed, when the object is close to the interface, strong interactions due to these resonances can be observed.

If the target is acoustically rigid, then both strengths have a shape of oscillation curves. The period of oscillations decreases as x increases. For the source contribution, the period of oscillations in ka is calculated as $2\pi a/\left(R_d - R\right)$. At x = 50 m, the periods obtained by this formula and from Figure 2 are equal to 1.02 (the difference is less than 10^{-3}).

The effect of the target scattered field contribution results in the shift of maximum values to higher frequencies at x = 10, 20 m and to lower frequencies at x = 30, 50 m. The amplitude of oscillations TS_{total} is larger than TS_{src} at x = 10, 20 m. At x = 30, 50 m, the situation is opposite. The difference between neighboring maximal and minimal values of TS_{total} and TS_{src} decreases as x increases.

The computational results are summarized in Table 1.

The dependences TS_{src} (dashed line) and TS_{total} (solid line) on distance x at ka = 58.4 (f = 46.47 kHz) and θ = 65° are shown in Figure 6. The periods of oscillations of these curves near x = 50 are the same and equal to 1.77 (the difference is less than 10^{-3}).

The dependencies TS_{total} on ka are calculated at other angles θ_s of the source location: θ_s = 30°, θ_s = 45°, θ_s = 65°; r_s = 100 m, R_{ref} = 100 m, and x = 50 m. The case θ_s = 90° is shown in Figure 2. The periods of oscillations of these curves in ka increase as the angle θ_s increases. These periods are equal to 0.05, 0.06, 0.11. At θ_s = 90°, the period of oscillations in ka is equal to 1.02 (Table 1). The maximal values of TS_{total} decrease as θ_s increases.

Table 1 Computational results for different locations of the receiver (coordinate x)

Compared parameters	Strength	x = 10	x = 20	x = 30	x = 50
Period of oscillations, in ka (in Hz)	Source	2.16 (1 716)	1.59 (1 266)	1.30 (1 038)	1.02 (809)
	Total	2.16 (1 721)	1.60 (1 273)	1.30 (1 036)	1.02 (810)
Maximal value near ka = 60, in dB	Source	0.46	−0.32	−1.04	−2.34
	Total	1.87	−0.06	−1.10	−2.62
Minimal value near ka = 60, in dB	Source	−2.36	−3.13	−3.84	−5.14
	Total	−4.73	−3.48	−3.70	−4.72
Difference between maximal and minimal values near ka = 60, in dB	Source	2.81	2.81	2.80	2.80
	Total	6.60	3.42	2.60	2.10
max TS_{total} − max TS_{src} near ka = 60, in ka (in Hz)		0.22 (179)	0.12 (94)	0.09 (72)	0.04 (30)

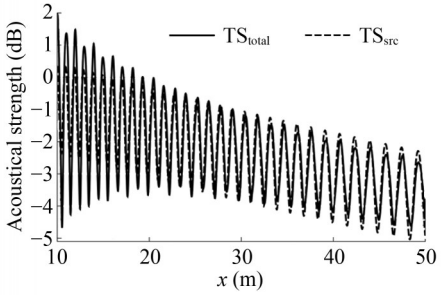

Figure 6 Dependence of the source strength TS_{src} (dashed line) and the total strength TS_{total} (solid line) on distance x, $10 \leqslant x \leqslant 50$ m at the frequency $f = 46.5$ kHz ($ka = 58.4$); $\theta = 65°$

In Figure 7, the dependences TS_{total} on ka are shown for $\theta_s = 45°$ (solid line) and $\theta_s = 65°$ (dashed line).

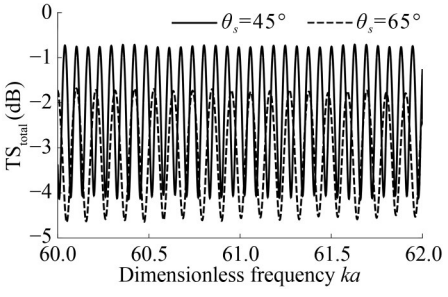

Figure 7 Dependence of the total strength TS_{total} on ka for the source located at the point $M_s(r_s, \theta_s, \pi)$, where $r_s = 100$ m and $\theta_s = 45°$ (solid line), and at the point M_s when $r_s = 100$ m, $\theta_s = 65°$ (dashed line). The receiver is located at the point $M(r, \theta, 0)$, where $r = 55.17$ m and $\theta = 65°$

4 Discussion of the obtained results

The efficient method for computing the far-field scattered by a spherical target near the seabed is proposed. The bottom is supposed to be a homogeneous liquid attenuating half-space. The transmitter and receiver are situated at different points of a homogeneous water half-space. The distances between the transmitter, receiver, and target are assumed to be much larger than the acoustic wavelength in water. Reciprocal locations of the transmitter, receiver, and target are unrestricted. In the computational example, the source and receiver are located on the different sides from the scattering sphere.

We follow Hackman and Sammelmann's general approach in calculating the far-field. The arising scattering coefficients of a sphere are evaluated using the steepest descent method. The use of the obtained asymptotic expressions also allows a decrease in the number of summands in the formula for the scatterer contribution to the total scattered field. For the numerical example investigated in this study at $f = 60$ kHz, the number of summands decreases from 4, 500 to 95 (by 45 times). Moreover, these summands only include elementary functions without their integration.

The computational examples demonstrate the efficiency of the presented technique. The total strengths calculated using the proposed technique and the exact values of total strengths calculated using (3)–(7) are compared at several points from the interval $55 \leqslant ka \leqslant 60$. At all these points, the difference between them is of the order of 10^{-3}. Thus, the agreement between the exact and asymptotic formulas is excellent.

The obtained asymptotic formula for the scatterer contribution can be used for the elastic target or the spherical elastic shell. In this case, it only requires replacing elements of the free-field T-matrix.

The computational examples show that the effect of the target scattered field contribution results in the shift of maximum values to higher frequencies. The amplitude of oscillations TS_{total} is larger than TS_{src} at $x = 10$, 20, 50 m. At $x = 30$, 50 m, the situation is opposite. The period of oscillations decreases as x increases.

5 Conclusions

This study presents an efficient method for computing the far-field scattered by a spherical target located near the seabed. Reciprocal locations of the transmitter, receiver, and target are unrestricted. In the computational example, the source and receiver are located on the different sides from the scattering sphere.

The technique is based on the evaluation of the arising scattering coefficients of a sphere with the use of the steepest descent method. The efficiency arises from the availability to significantly reduce the number of summands in the formula for the scatterer contribution to the total scattered field. In addition, the integrals, which have slowly decreasing and rapidly oscillating integrands, can be substituted with expressions that involve only elementary functions.

The obtained formulas for the target strength can be used for acoustically rigid or soft scatterers, as well as elastic targets or spherical elastic shells. Numerical simulations are conducted for an acoustically rigid sphere. Asymptotic expressions for the scattering coefficients allow a decrease in the number of summands in the formula for the target strength and a significant reduction in computational time.

Funding Supported by the Ministry of Science and Higher Education of the Russian Federation as a part of World-class Research Center Program: Advanced Digital Technologies (contract No. 075-15-2022-312 dated 20 April 2022).

Competing interest The authors have no competing interests to declare that are relevant to the content of this article.

References

Bateman H, Erdélyi A (1953) Higher transcendental functions; McGraw-Hill Book Company, New York, Vol 1, 125-170

Brekhovskikh LM (1980) Waves in layered media. 2nd edn, Academic Press, New York

Brekhovskikh LM, Godin OA (1990) Acoustic of Layered Media I: Plane and Quasi-Plane Waves. 1st edn. Springer Berlin/Heidelberg. https://doi.org/10.1007/978-3-642-52369-4

Brekhovskikh LM, Godin OA (1999) Acoustic of Layered Media II: Point Sources and Bounded Beams. 2nd edn, Springer Berlin/Heidelberg. https://doi.org/10.1007/978-3-662-03889-5

Fawcett JA (2000) Complex-image approximations to the half-space acousto-elastic Green's function. J Acoust Soc Am 108: 2791-2795. https://doi.org/10.1121/1.1322024

Fawcett JA (2003) A method of images for a penetrable acoustic waveguide. J Acoust Soc Am 113: 194-204. https://doi.org/10.1121/1.1523082

Fawcett JA, Fox WL, Maguer A (1998) Modeling of scattering by objects on the seabed. J Acoust Soc Am 104: 3296-3304. https://doi.org/10.1121/1.423969

Fawcett JA, Lim R (2003) Evaluation of the integrals of target/seabed scattering using the method of complex images. J Acoust Soc Am 114: 1406-1415. https://doi.org/10.1121/1.1600726

Gaunaurd GC, Huang H (1994) Acoustic scattering by a spherical body near a plane boundary. J Acoust Soc Am 96: 2526-2536. https://doi.org/10.1121/1.410126

Gaunaurd GC, Huang H (1995) Acoustic scattering by an air-bubble near the sea surface. IEEE J Ocean Eng 20: 285-292. https://doi.org/10.1109/48.468253

Grigorieva NS, Fridman GM (2013) Scattering of sound by an elastic spherical shell immersed in a waveguide with a liquid bottom. Acoust Phys 59: 373-381. https://doi.org/10.1134/S1063771013040064

Grigorieva NS, Kupriyanov MS, Mikhailova DA, Ostrovskiy DB (2016) Sound wave scattering by a spherical scatterer located near an ice surface. Acoust Phys 62: 8-21. https://doi.org/10.1134/S1063771016010036

Grigorieva NS, Legusha FF, Nikushchenko DV, Safronov KS (2023) Interference of echo-signals from two buried spherical targets. MPDI: Acoustics 5: 509-521. https://doi.org/10.3390/acoustics5020030

Hackman RH, Sammelmann GS (1986) Acoustic scattering in an inhomogeneous waveguide: Theory. J Acoust Soc Am 80: 1447-1458. https://doi.org/10.1121/1.394400

Hackman RH, Sammelmann GS (1988) Multiple-scattering analysis for a target in an oceanic waveguide. J Acoust Soc Am 84: 1813-1825. https://doi.org/10.1121/1.397148

Hickling R (1964) Analysis of echoes from a hollow metallic sphere in water. Acoust Soc Am 36: 1124-1137. https://doi.org/10.1121/1.1919173

Huang H, Gaunaurd GC (1996) Acoustic point source scattering by a spherical elastic shell submerged beneath a free surface. J Acoust Soc Am 99: 2720-2726. https://doi.org/10.1121/1.414814

Kargl SG, Marston PL (1990) Ray synthesis of Lamb wave contribution to the total scattering cross section for an elastic spherical shell. J Acoust Soc Am 88: 1103-1113. https://doi.org/10.1121/1.399806

Nobile MA, Hayek SI (1985) Acoustic propagation over an impedance plane. J Acoust Soc Am 78: 1325-1336. https://doi.org/10.1121/1.392902

Ochmann M (2004) The complex equivalent source method for sound propagation over an impedance plane. J Acoust Soc Am 116: 3304-3311. https://doi.org/10.1121/1.1819504

Sessarego JP, Cristini P, Grigorieva NS, Fridman GM (2012) Acoustic scattering by an elastic spherical shell near the seabed. J Comput Acoust 20: 1250006. https://doi.org/10.1142/S0218396X12500063

Taraldsen G (2005) The complex image method. Wave Motion 43: 91-97. https://doi.org/10.1016/j.wavemoti.2005.07.001

Zampolli M, Jensen FB, Tesei A (2009) Benchmark problems for acoustic scattering from elastic objects in the free field and near the seafloor. J Acoust Soc Am 125: 89-98. https://doi.org/10.1121/1.3027446

Zampolli M, Tesei A, Canepa G, Godin OA (2008) Computing the far field scattered or radiated by objects inside layered fluid media using approximate Green's functions. J Acoust Soc Am 123: 4051-4058. https://doi.org/10.1121/1.2902139